Model-Based Segmentation of Pathological Lungs in Volumetric CT Data

Shanhui Sun[1,5], Geoffrey McLennan[2,3,4,5], Eric A. Hoffman[3,2,4,5], and Reinhard Beichel[1,2,5]

[1] Dept. of Electrical and Computer Engineering
[2] Dept. of Internal Medicine
[3] Dept. of Radiology
[4] Dept. of Biomedical Engineering
[5] The Iowa Institute for Biomedical Imaging
The University of Iowa, Iowa City, IA 52242, USA
reinhard-beichel@uiowa.edu

Abstract. Segmentation of pathological lungs is a non-trivial problem. We present a new approach for the segmentation of lungs with high-density pathologies like lung cancer. Our method consists of two main processing steps. First, a novel robust active shape model matching method is applied to roughly segment the outline of the lungs. Second, an optimal surface finding approach is utilized to refine the initial segmentation result. Left and right lungs are segmented separately. A comparison to an independent reference on eleven abnormal (lung cancer) and nine normal test cases resulted in an average Dice coefficient of 0.9741 and 0.9758, respectively. Our algorithm was specifically designed for general-purpose computation on graphics processing units (GPGPU) and requires on average 116 seconds for segmenting a left or right lung.

1 Introduction

Many computer-aided lung image analysis methods require the segmentation of lung tissue in an initial processing step. In the case of normal lungs imaged with X-ray computed Tomography (CT), lung segmentation is a rather simple task because of the large density difference between air-filled lung tissue and surrounding tissues. Many algorithms can be found in the literature that deal with the segmentation of normal lungs [1–5]. In the case of lungs with high density pathology (e.g., cancer, pneumonia, etc.) as shown in Fig. 1(a), segmentation becomes a non-trivial problem and conventional algorithms fail to deliver correct segmentation results (Fig. 1(b)). Pathological cases are frequently occurring in clinical practice and constitute the crucial cases for computer-aided diagnosis and treatment planning/monitoring.

There is scant literature about robust lung segmentation methods. Sluimer et al. propose a segmentation by registration scheme in which scans of normal lungs are elastically registered to a scan with pathology [6]. While delivering promising results, not all pathological cases could be handled successfully [6].

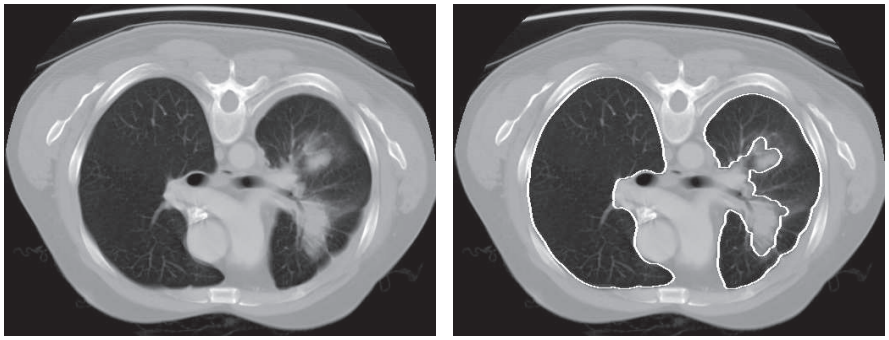

(a) (b)

Fig. 1. Lung segmentation. (a) Axial CT image showing normal right and pathological (cancer) left lung tissue and (b) corresponding segmentation result generated with a standard lung segmentation method.

In addition, the authors also identified the need to reduce the time needed by the registration algorithm from three hours to a clinically more acceptable processing time [6]. To address this problem, a hybrid lung segmentation method was presented in a recent publication [7]. The idea is to first use a fast conventional lung segmentation algorithm followed by a segmentation error detection step. If errors are detected, the more complex algorithm is utilized. An adaptive border marching algorithm was presented in [8] to include juxtapleural nodules in lung segmentations. Larger areas of under-segmentation were reported in hilar and pulmonary consolidation regions [8]. A combination of a Bézier surface model for the side walls of lungs and a conventional lung segmentation technique was proposed in [9] to deal with lesions located at the lung border. An approach for the robust segmentation of lung parenchyma based on the curvature of ribs was presented in [10]. The method is based on an adaptive thresholding scheme and utilizes a comparison of the curvature of the lung boundary to the curvature of the ribs to select thresholds. Because lung pathologies like cancer can have density values similar to other tissues surrounding the lung, the method will likely produce errors in such cases.

In this paper we present a new approach for the segmentation of lungs with high-density lung disease (e.g., cancer, fibrosis, pneumonias, etc.) that addresses limitations of existing methods like robustness or processing speed. Our approach is based on a lung model and utilizes a novel robust model matching method. To be suitable for routine application, the time required for lung segmentation must be low. The model-based 3D segmentation of lungs is particular challenging, because of the size of lungs and the amount of image data to be processed. Our approach to robust lung segmentation addresses this issue—the algorithm is specifically designed to take advantage of general-purpose computation on graphics processing hardware, which reduces the execution time considerably.

2 Methods

In the following Sections, we describe the individual processing steps of our robust lung segmentation approach.

2.1 Lung Model Generation

To represent lung shapes, a model describing the mean shape and variation around the mean was generated. For this purpose, $n = 41$ segmented normal lung CT data sets imaged at total lung capacity (TLC) were used, and a set of corresponding landmarks $\{\mathbf{s}_1, \mathbf{s}_2, \ldots, \mathbf{s}_m\}$ with $m = 2562$ were identified on all lung shapes by means of minimum description length (MDL) approach [11]. All n landmark sets were aligned into a common coordinate frame by using procrustes analysis, resulting in a mean shape vector $\bar{\mathbf{x}}$. For each learning shape, a shape vector $\mathbf{x}_i$ with $i = 1, 2, \ldots, m$ was generated by concatenating the coordinates: $\mathbf{x}_i = [x_{i,1}, y_{i,1}, z_{i,1}, x_{i,2}, y_{i,2}, z_{i,2}, \ldots, x_{i,m}, y_{i,m}, z_{i,m}]^T$. A principal component analysis (PCA) was applied to generate a point distribution model (PDM) [12]. The above outlined process was applied to left and right lungs, yielding independent left and right lung PDMs. An instance of a left or right lung shape can be generated from the corresponding PDM by the linear model: $\mathbf{x} = \bar{\mathbf{x}} + \mathbf{P}\mathbf{b}$, where $\mathbf{P}$ denotes the shape eigenvector matrix and $\mathbf{b}$ represents the shape coefficients.

2.2 Robust Active Shape Model Matching

a) Standard Matching Scheme The PDM described in the previous Section can be used for lung segmentation by matching the model to the target structure. This could be accomplished by utilizing a standard active shape model (ASM) matching framework [12]. First, an instance of the shape model (e.g., mean shape) is generated and placed in proximity to the target structure in the image volume. Second, to match the model, shape points are updated by searching from the current landmark position along a profile of length l_{ASM} perpendicular to the model surface. To identify suitable update points $\mathbf{y}$, we use the following cost function $c_i = g_{mag_i}$, and update point locations with $\boldsymbol{n}_i \cdot \boldsymbol{g}_{dir_i} < 0$ are ignored. c_i represents the cost of the i-th column element, and the associated sampled gradient magnitude, gradient direction, and normal vector are denoted as g_{mag_i}, $\boldsymbol{g}_{dir_i}$, and $\boldsymbol{n}_i$, respectively. The gradient calculation is based on Gaussian derivatives with a standard deviation of σ_{ASM}, and the calculation of $\boldsymbol{g}_{dir}$ and g_{mag} is done for each voxel of the volume before the model matching is started. These pre-calculated gradient values are then used to interpolate gradient vectors during model matching. If a gradient value outside the volume is required during model matching, a value closest to the boundary is utilized. In case that no new update point can be found, the old position is used.

Once all shape points are updated, pose parameters are adjusted to map the updated shape points to the mean model. For this purpose, a procrustes alignment step is used to estimate transformation matrix $\mathbf{T}$, which consists of

scaling, rotation, and translation parameters, by minimizing $(\mathbf{T}[\mathbf{y}] - \bar{\mathbf{x}})^T(\mathbf{T}[\mathbf{y}] - \bar{\mathbf{x}})$. Model parameters $\mathbf{b}$ are updated by using

$$\mathbf{b} = \mathbf{P}^T(\mathbf{T}[\mathbf{y}] - \bar{\mathbf{x}}) \; . \tag{1}$$

The outlined process is repeated until the model converges.

We are especially interested in the segmentation of pathological lungs that contain areas of lung disease with high density (e.g., pneumonia, cancer, etc.). Thus, it is very likely that some update points are found during the model matching procedure that do not represent lung surface and belong to an area of transition between normal and diseased lung tissue. Consequently, the standard matching approach will fail, since it is a least squares optimization procedure that is not suitable to handle outliers. Therefore, a robust shape model matching approach is needed.

b) Robust Matching Approach The basic idea behind robust ASM matching is to only use inlier components of $\mathbf{y}$ to update model parameters. In this context, Rogers et al. investigated M-estimators and random sampling-based robust parameter estimation techniques for 2D ASM matching [13]. It is well known that the effectiveness of M-estimators strongly depends on the selection of the weighting function and its parameters. Usually, this selection is not trivial, and the optimal selection might change from case to case. Random sampling techniques try to find a subset of inliers by evaluating a number of randomly sampled subsets of update points. Such approaches work well, if the required subset of inliers is quite small. In case of large ASM models, this strategy can lead to suboptimal results, because a small set of inliers might not be representative enough to describe a complex lung shape (many landmark points), and thus can negatively impact the matching result. For our application, it is desirable to use as many inliers as possible for the model update.

In the following, we present a new robust ASM matching algorithm that extends the standard matching approach (Section 2.2.a) by an outlier detection step. For this purpose, we use a robust PCA coefficient estimation scheme that builds on the work of Storer et al. [14]. The method presented in [14] was designed for robust image reconstruction and targets a pre-defined number of inliers. In this paper, we propose a novel voting scheme that does not require to specify a targeted number of inliers. Our method consists of two processing steps. First, normal shape patterns of landmark subsets are learned. Second, these patterns are then utilized during ASM matching to identify and reject outliers.

i) Offline learning Corresponding landmark points of all learning shapes are partitioned randomly into k shape subsets of approximately equal size. This process is repeated l-times, resulting in a set of subsets: $\Omega = \{\omega_{i,j} | i \in 1, 2, \ldots, l, \;\; j \in 1, 2, \ldots, k\}$. Note that corresponding landmark points of all n learning data sets are always assigned to the same subset. Consequently, each subset $\omega_{i,j}$ consists of n subset samples. For each subset $\omega_{i,j}$, a mean shape $\bar{\mathbf{x}}_{\omega_{i,j}}$ is calculated by using procrustes analysis, and all shapes of the subset are aligned. The subset shapes are then converted to shape vectors by concatenating

their x-, y-, and z-components. By means of PCA, the corresponding eigenvectors $\mathbf{P}_{\omega_{i,j}}$ are calculated. $\bar{\mathbf{x}}_{\omega_{i,j}}$ and $\mathbf{P}_{\omega_{i,j}}$ are stored and will be utilized for robust ASM matching.

ii) Robust matching To robustly match the model to image data, we must identify outliers in the update point vector $\mathbf{y}$ in each iteration. This is accomplished by analyzing subset combinations of $\mathbf{y}$ and by utilizing a voting scheme. Let $\mathbf{y}_{\omega_{i,j}}$ represent the components of $\mathbf{y}$ that are corresponding to the landmark points that constitute subset $\omega_{i,j}$. For each subset, a reconstruction error $e_{\omega_{i,j}} = \left\| \mathbf{T}_{\omega_{i,j}}[\mathbf{y}_{\omega_{i,j}}] - \left[\bar{\mathbf{x}}_{\omega_{i,j}} + \mathbf{P}_{\omega_{i,j}} \tilde{\mathbf{b}}_{\omega_{i,j}} \right] \right\|$ is calculated, where $\mathbf{T}_{\omega_{i,j}}$ is a transformation matrix that aligns $\mathbf{y}_{\omega_{i,j}}$ to the corresponding mean $\bar{\mathbf{x}}_{\omega_{i,j}}$. The vector $\tilde{\mathbf{b}}_{\omega_{i,j}}$ is derived from $\mathbf{b}_{\omega_{i,j}} = \mathbf{P}^T_{\omega_{i,j}} \left[\mathbf{T}_{\omega_{i,j}}[\mathbf{y}_{\omega_{i,j}}] - \bar{\mathbf{x}}_{\omega_{i,j}} \right]$ by limiting the components of the parameter vector $\mathbf{b}_{\omega_{i,j}}$ to a value of $\pm\xi$-times the square-root of the corresponding eigenvalue.

A large reconstruction error $e_{\omega_{i,j}}$ is an indication that subset $\omega_{i,j}$ is very likely contaminated by one or more outliers. To identify the outliers, the reconstruction error $e_{\omega_{i,j}}$ is interpreted as a vote, which is casted for all update points that are included in the subset $\mathbf{y}_{\omega_{i,j}}$. This voting process is carried out for all subsets $\omega_{i,j} \in \Omega$. The casted votes are collected in a matrix $\mathbf{V}_{err}$ of size $m \times l$, in which rows correspond to shape points in $\mathbf{y}$. After all votes are casted, $\mathbf{V}_{err}$ is analyzed to detect outliers. First, to increase robustness, a rank order statistics filter is applied to each row; the values are sorted, and the g-lowest value is selected to represent the filter result. The filtering step reduces $\mathbf{V}_{err}$ to a vector $\mathbf{v}_{err} = [v_1, v_2, \ldots, v_m]^T$ and helps to reject accidental occurring point constellations that contain outliers, which are similar to constellations of inlier points. Second, a threshold δ is derived from $\mathbf{v}_{err}$ by analyzing the distribution of vector components v_i: $\delta = \mu + \beta\sigma$ with $\mu = median_{i \in 1,2,\ldots,m}\{v_i\}$ and $\sigma = \sqrt{1/m \sum_{i=1}^{m} (v_i - \mu)^2}$, where β represents a constant. If needed, this step can be replaced by a more advanced mean shift-based analysis step, similar to the approach reported in [15]. Third, the threshold is applied to $\mathbf{v}_{err}$ to yield a selection vector: $\mathbf{p}_{sel} = [p_1, p_2, \ldots, p_m]^T$ with

$$p_i = \begin{cases} 1 : v_i < \delta \\ 0 : v_i \geq \delta \end{cases} \tag{2}$$

to discriminate between inliers ($p_i = 1$) and outliers ($p_i = 0$). Once the inliers are identified, an update of the model parameter vector is calculated by utilizing a modified version of Eq. 1 which takes $\mathbf{p}_{sel}$ into account. An advantage of our outlier detection algorithm is that it is well suited for parallel processing. For example, we utilize a general-purpose computing on graphics processing units (GPGPU) implementation.

For our application, we used the following parameters: $l_{ASM} = \pm 40$ mm, $k = 200$, $l = 60$, $\xi = 2$, $g = 10$, and $\beta = 1.3$. To update the robust ASM, a gradient image was calculated based on Gaussian derivatives with a standard deviation of $\sigma_{ASM} = 4$. The maximum gradient position along the search profile was used to calculate updates for shape points. The maximum number of iterations during

model matching was set to 100, and model matching was stopped if the average of the shape point movement was below 0.04 mm.

2.3 Model Constrained Optimal Surface Finding

Depending on the training data utilized for model building, the model might not be able do describe smaller local shape variations. To capture this information, we generate the final lung segmentation by applying a global optimal surface finding method [16]. The algorithm transforms the segmentation problem into a graph optimization problem, which is solved by means of a maximum-flow algorithm [16]. Thus, an edge-weighted directed graph is built, and weights derived from the volume are assigned to the graph edges to reflect local image properties. For this purpose, the final ASM mesh is utilized. Since the ASM vertices are sparse, the mesh is restructured by adding triangles, before the graph is built. For graph generation, columns along the surface normal of each vertex (search profile) are generated. The length l_p of the profile is utilized to constrain the segmentation to the proximity of the initial ASM segmentation. In addition, a surface smoothness constraint Δ is incorporated into the graph as described in [16]. For segmentation we use the following cost function:

$$c_i = \begin{cases} g_{max} & if\ \boldsymbol{n}_i \cdot \boldsymbol{g}_{dir\,i} < 0 \\ g_{max} - g_{mag_i} & otherwise \end{cases}, \tag{3}$$

where c_i represents the cost of the i-th column element and g_{max} the maximum gradient magnitude of the volume. The gradient calculation is based on Gaussian derivatives with a standard deviation of σ_g. We utilize the optimal surface finding in an iterative fashion, and the used sequence of values for σ_g and Δ was $\{6.0, 3.0, 1.0, 0.5\}$ and $\{10, 8, 5, 2\}$, respectively. For the search profile, $l_p = \pm 10$ voxel was selected.

3 Case Studies

To evaluate the performance of our method, 20 segmentations were performed on 10 multidetector computed tomography (MDCT) scans (Fig. 2). For each data set, left and right lungs were segmented, and either the left and/or right lung contained diseased lung tissue with a significant higher density compared to normal tissue. The image size varied from $512 \times 512 \times 458$ to $512 \times 512 \times 572$ voxel. The in-plane resolution of the images ranged from 0.580×0.580 to 0.809×0.809 mm and the slice thickness from 0.6 to 0.7 mm. To generate an independent reference standard, a reference segmentation of left and right lungs was generated by an expert for all 10 scans. This process took several hours per case.

The initialization of the model was done manually by placing the corresponding left or right mean shape model with a fixed size in the individual data sets. For each method investigated in this paper, the same starting position and initial shape was used.

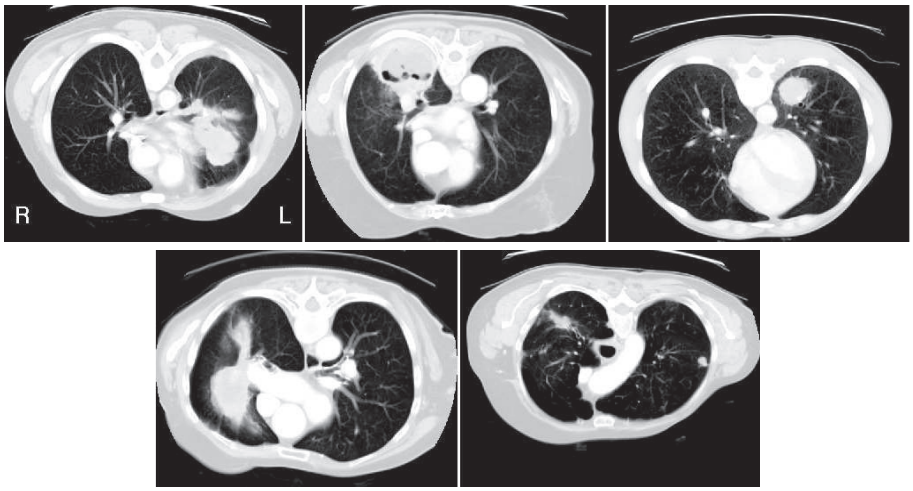

Fig. 2. Examples of lung data sets with high-density pathology that were utilized for evaluation of our approach. From left to right and top to bottom: hdl01, hdl03, hdl04, hdl07, and hdl10.

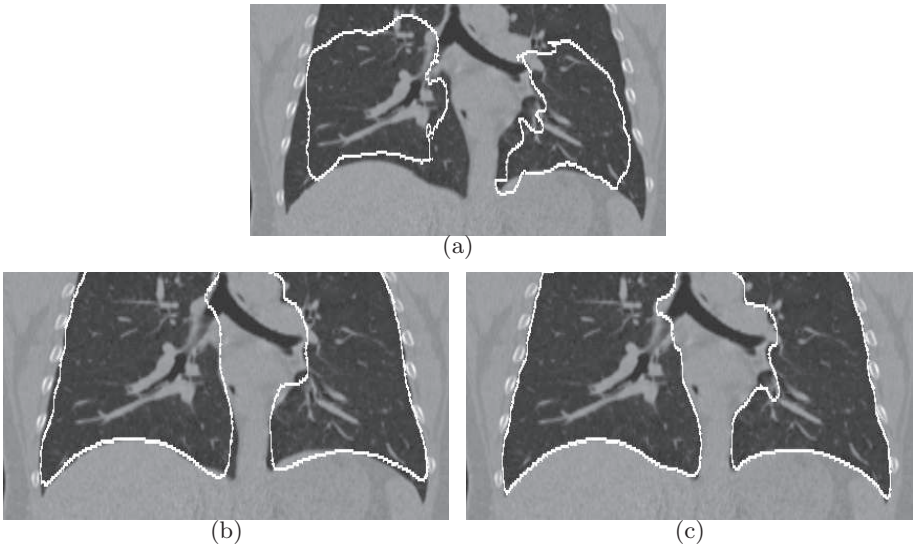

(a) (b) (c)

Fig. 3. Segmentation of an incomplete lung CT data set; the top portion was not scanned. (a) Standard ASM. (b) Robust ASM. (c) Combination of robust ASM and optimal surface finding. Note that the standard and robust ASMs are not aware of the spatial extent of the data set, because of the clamping of gradient values to the boundary (Section 2.2.a). Surfaces outside of the data set were clipped after the segmentation process was completed.

Segmentation results obtained with a standard ASM, our robust ASM, and the proposed approach (robust ASM and optimal surface finding (OSF) combined) are summarized in Table 1. To quantify segmentation performance, the Dice coefficient $D(S,R) = 2(|S \cap R)/(|S| + |R|)$ was calculated, where S represents the segmentation and R the reference.

On average, 115 seconds and 116 seconds were required by our robust lung segmentation method for right and left lung segmentation, respectively. The average time required for the intrinsic robust ASM matching process was 24 seconds. All computations were performed on a standard workstation equipped with a NVIDIA Tesla C1060 Computing Processor.

To assess the robustness of our approach, we applied our method to a CT data set where the top of the lung was not imaged (Fig. 3(b) and 3(c)). For comparison, the standard ASM result is depicted in Fig. 3(a). Figs. 1 and 4 allow us to compare our segmentation approach with a clinically used lung segmentation method.

4 Discussion and Conclusion

The experiments presented in Section 3 demonstrate the ability of our lung segmentation method to successfully deal with high-density lung pathology (Fig. 4) or other disturbances (Fig. 3). Our robust ASM matching clearly outperforms the standard ASM approach (Table 1). Even on normal lungs, the standard ASM delivers inferior performance. Pathologies like lung masses degrade matching performance even further, as demonstrated by the results in Table 1. These results are not surprising, because (standard) ASM matching is a least squares optimization, which is sensitive to outliers. Since the model is only roughly placed in proximity to the lung during initialization, all obstacles between model and target structure can cause problems.

The optimal surface finding step after robust ASM segmentation allows us to refine the robust ASM result. This step is needed, because our shape model was built from only 41 data sets, and consequently, some local shape variations cannot be explained by the model. In our final segmentation results, major deviation from the reference were observed in regions where airways and pulmonary vessels enter/leave the lung. Even for experts, it is hard to segment this area consistently.

So far, we have tested our robust lung segmentation method on lung cancer cases. In the future, we plan to significantly enlarge our training and test data set to include instances of fibrosis, pneumonia, etc. Our approach is currently limited to scans acquired at TLC. We plan to address this issue by developing a 4D lung model.

A method for the segmentation of lungs with high-density pathology was presented and evaluated on lung cancer cases. The robustness of our approach was demonstrated in 20 experiments, and a low segmentation error was achieved in cases with and without high-density pathology. A core component of our

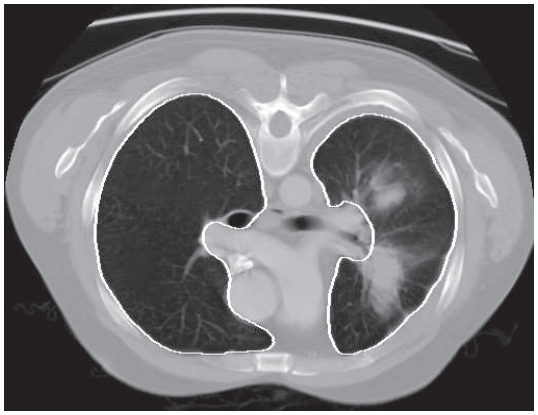

Fig. 4. Robust lung segmentation. Example shown in Fig. 1(a) segmented with the proposed robust lung segmentation approach.

method is a novel robust ASM matching approach that is well suitable for large shape models and is general applicable.

Our method for robust lung segmentation opens up new avenues for computer-aided lung image analysis. For example, segmentation of diseased lungs and segmentation of the diseased tissue itself are related problems. Thus, we expect that our method will be of significant benefit for the quantification of lung diseases.

Conflict of interest statement: Eric Hoffman and Geoffrey McLennan are founders and share holders of VIDA Diagnostics, a company which is commercializing lung image analysis software.

References

1. Armato, S.G., Sensakovic, W.F.: Automated lung segmentation for thoracic CT. Acad. Radiol. **11**(9) (2004) 1011–1021
2. Leader, J.K., Zheng, B., Rogers, R.M., Sciurba, F.C., Perez, A., Chapman, B.E., Patel, S., Fuhrman, C.R., Gur, D.: Automated lung segmentation in X-ray computed tomography. Acad. Radiol. **10**(11) (2003) 1224–1236
3. Silva, A., Silva, J.S., Santos, B.S., Ferreira, C.: Fast pulmonary contour extraction in X-ray CT images: a methodology and quality assessment. In: Proc. SPIE (Medical Imaging). Volume 4321. (2001) 216–224
4. Hu, S., Hoffman, E.A., Reinhardt, J.M.: Automatic lung segmentation for accurate quantitation of volumetric X-ray CT image. IEEE Trans. Med. Imag. **20**(6) (2001) 490–498
5. Hoffman, E.A., Sinak, L.J., Robb, R.A., Ritman, E.L.: Noninvasive quantitative imaging of shape and volume of lungs. Journal of Applied Physiology **54**(5) (1983) 1414–1421
6. Sluimer, I., Prokop, M., van Ginneken, B.: Toward automated segmentation of the pathological lung in CT. IEEE Trans. Med. Imag. **24**(8) (2005) 1025–1038

Case	Dice Coefficient					
	Right Lung			Left Lung		
	ASM	RASM	RASM+OSF	ASM	RASM	RASM+OSF
hdl01	0.9274	0.9549	0.9806	**0.8438**	**0.9301**	**0.9685**
hdl02	**0.8399**	**0.9436**	**0.9753**	0.8422	0.9453	0.9746
hdl03	**0.7456**	**0.9098**	**0.9606**	0.8505	0.9364	0.9724
hdl04	0.9071	0.9557	0.9761	**0.8473**	**0.9372**	**0.9686**
hdl05	**0.8368**	**0.9356**	**0.9707**	0.8490	0.9446	0.9741
hdl06	**0.9117**	**0.9600**	**0.9820**	0.8652	0.9440	0.9798
hdl07	**0.8117**	**0.9338**	**0.9824**	0.8007	0.9222	0.9751
hdl08	0.9315	0.9499	0.9800	**0.7836**	**0.9349**	**0.9768**
hdl09	**0.8810**	**0.9639**	**0.9785**	0.7571	0.9346	0.9699
hdl10	**0.9197**	**0.9425**	**0.9742**	**0.8505**	**0.9395**	**0.9775**
mean	0.8712	0.9450	0.9760	0.8290	0.9369	0.9737

Table 1. Lung segmentation results for standard ASM (ASM), robust ASM (RASM), and proposed (RASM+OSF) approach. Bold numbers represent cases with high-density pathology.

7. van Rikxoort, E., de Hoop, B., Viergever, M., Prokop, M., van Ginneken, B.: Automatic lung segmentation from thoracic computed tomography scans using a hybrid approach with error detection. Medical Physics **36** (2009) 2934–2947
8. Pu, J., Roos, J., Yi, C.A., Napel, S., Rubin, G.D., Paik, D.S.: Adaptive border marching algorithm: Automatic lung segmentation on chest CT images. Computerized Medical Imaging and Graphics **32**(6) (2008) 452 – 462
9. Kitasaka, T., Mori, K., Hasegawa, J., Toriwaki, J.: Lung area extraction from 3D chest X-ray CT images using a shape model generated by a variable Bézier surface. Systems and Computers in Japan **34**(4) (2003) 60–71
10. Prasad, M.N., Brown, M.S., Ahmad, S., Abtin, F., Allen, J., da Costa, I., Kim, H.J., McNitt-Gray, M.F., Goldin, J.G.: Automatic segmentation of lung parenchyma in the presence of diseases based on curvature of ribs. Academic Radiology **15**(9) (2008) 1173 – 1180
11. Heimann, T., Wolf, I., Williams, T., Meinzer, H.P.: 3D active shape models using gradient descent optimization of description length. In: In Proc. IPMI. Volume 3565., Springer, Heidelberg (2005) 566–577
12. Cootes, T.F., Cooper, D., Taylor, C.J., Graham, J.: Active shape models - their training and application. Computer Vision and Image Understanding **61**(1) (1995) 38–59
13. Rogers, M., Graham, J.: Robust active shape model search. In: In Proceedings of the European Conference on Computer Vision, Springer (2002) 517–530
14. Storer, M., Roth, P., Urschler, M., Bischof, H.: Fast-robust PCA. In: 16th Scandinavian Conference on Image Analysis. (2009) 430–439
15. Beichel, R., Bischof, H., Leberl, F., Sonka, M.: Robust active appearance models and their application to medical image analysis. IEEE Trans. Med. Imag. **24**(9) (2005) 1151–1169
16. Li, K., Wu, X., Chen, D., Sonka, M.: Optimal surface segmentation in volumetric images - a graph-theoretic approach. IEEE Trans. Pattern Anal. Mach. Intell. **28**(1) (2006) 119–134